International Journal of Pharmaceutics 702 (2026) 127207

Contents lists available at ScienceDirect

International Journal of Pharmaceutics

journal homepage: www.elsevier.com/locate/ijpharm

Liposomes versus Sphingosomes: Microfluidic DoE-Guided development of lipid nanocarriers for the delivery of a synthetic hMAO inhibitor

Giorgio Buttitta [a,*], Michele Coluccia [a], Simone Bonacorsi [b], Francesca Diomede [c], Guya Diletta Marconi [c], Jacopo Pizzicannella [c], Elena De Falco [d,e], Paolo Guglielmi [a]

[a] Department of Drug Chemistry and Technologies, "Sapienza" University of Rome, Rome, Italy
[b] BSP Pharmaceuticals, Via Appia, km. 65, 561 04100 Latina LT, Italy
[c] Department of Innovative Technologies in Medicine & Dentistry, "G. d'Annunzio" University of Chieti-Pescara, Chieti, Italy
[d] Department of Medico-Surgical Sciences and Biotechnologies, Sapienza University of Rome, Latina, Italy
[e] Maria Cecilia Hospital, Gruppo Villa Maria Care & Research, Cotignola, Italy

ARTICLE INFO

Keywords:
Sphingosomes
Liposomes
DoE
Microfluidics
hMAO
Nanomedicine

ABSTRACT

Human monoamine oxidases (hMAO) are mitochondrial flavoenzymes responsible for the oxidative deamination of endogenous and exogenous amines, including key neurotransmitters. Their dysregulation has been associated with the onset and progression of neuropsychiatric and neurodegenerative disorders, such as depression and Parkinson's disease. Although pharmacological inhibition of hMAO represents a well-established therapeutic strategy, currently available inhibitors still present limitations, highlighting the need for both novel active compounds and advanced formulation approaches to improve their therapeutic performance.

In this study, two lipid-based nanocarrier systems, namely phosphatidylcholine-based liposomes and sphingomyelin-based vesicles (sphingosomes), were developed for the delivery of BT12, a promising novel benzo[b]thiophene-derived hMAO inhibitor characterized by extremely low aqueous solubility. A microfluidic approach combined with a multi-step Design of Experiments (DoE) strategy was employed to design and optimize both formulations. In this context, the systematic DoE strategy enabled the identification of critical process parameters influencing key quality attributes, including particle size, polydispersity index, and theoretical encapsulation efficiency. The optimized formulations (size < 100 nm; PDI ≈ 0.2) exhibited comparable physicochemical and morphological properties, as well as good colloidal stability under refrigerated conditions and in biologically relevant media. While sphingosomes showed a comparatively higher theoretical encapsulation efficiency ($35.8 \pm 1.1\%$) compared to liposomes ($20.4 \pm 0.7\%$), in vitro release studies demonstrated controlled and sustained release profiles for both systems over 72 h, with sphingosomes displaying slower release kinetics. Biological evaluation on SH-SY5Y neuronal-like cells indicated that both formulations were well tolerated, with liposomes exhibiting slightly higher cytocompatibility. Confocal microscopy of fluorescently labeled nanoparticles confirmed efficient cellular association and/or uptake for both systems, with no evident differences between formulations. Overall, these findings highlight the role of lipid composition in modulating nanocarrier performance, revealing a balance between comparatively greater BT12 retention and cytocompatibility, and supporting the rational design of lipid-based delivery systems for poorly water-soluble hMAO inhibitors.

Abbreviations: AD, Alzheimer's disease; BBB, blood brain barrier; BT12, Benzo[*b*]thiophen-2-yl(4-nitrophenyl)methanone; Chol, cholesterol; CQAs, critical quality attributes; CNS, central nervous system; CPPs, critical process parameters; DLS, dynamic light scattering; DoE, design of experiments; DSPE-PEG2000, 1,2-distearoyl-*sn*-glycero-3-phosphoethanolamine-*N*-[methoxy (polyethylene glycol)-2000] ammonium salt 18:0; ESM, sphingomyelin from egg; EtOH, ethanol; FRR, flow rate ratio; HBS, human blood serum; HEPES, 4-(2-hydroxyethyl)-1-piperazineethanesulfonic acid; hMAO, human monoamine oxidases; HPLC, high-performance liquid chromatography; HSPC, hydrogenated soy phosphatidylcholine; PD, Parkinson's disease; PBS, Phosphate buffered saline; PDI, polydispersity index; R^2, coefficient of determination.

* Corresponding author.
E-mail address: giorgio.buttitta@uniroma1.it (G. Buttitta).

https://doi.org/10.1016/j.ijpharm.2026.127207
Received 15 May 2026; Received in revised form 17 July 2026; Accepted 17 July 2026
Available online 22 July 2026

1. Introduction

Human monoamine oxidases (hMAO) are mitochondrial flavoenzymes responsible for the oxidative deamination of endogenous and exogenous amines, including key neurotransmitters such as dopamine, serotonin, and norepinephrine (Tipton, 2018). Two isoforms, hMAO-A and hMAO-B, differ in substrate specificity and physiological role, collectively contributing to the regulation of neurotransmitter homeostasis in the central nervous system (Iacovino et al., 2018). Beyond neurotransmitter turnover, hMAO activity leads to the production of hydrogen peroxide and reactive metabolites, which have been implicated in oxidative stress and neuronal damage. Consequently, dysregulation of hMAO activity has been associated with the onset and progression of both neuropsychiatric and neurodegenerative disorders, including depression and Parkinson's disease (PD), collectively contributing to a major global health burden (Rahman et al., 2021; Santin et al., 2021). Pharmacological inhibition of hMAO is a well-established therapeutic strategy. Selective hMAO-A inhibitors, such as moclobemide, are used in the treatment of depressive disorders (Burkard et al., 1989), whereas hMAO-B inhibitors, including selegiline and safinamide, are widely employed in the management of Parkinson's disease (Naoi et al., 2022). Despite their clinical relevance, currently available hMAO inhibitors present limitations related to pharmacokinetics, bioavailability, and dose-dependent adverse effects, which may restrict their therapeutic window and long-term use (Junkes et al., 2025; Kim et al., 2025). These challenges highlight the need for both the development of new active compounds and the implementation of formulation strategies capable of improving their therapeutic performance. In this context, recent medicinal chemistry efforts have led to the identification of novel compounds as hMAO inhibitors (Guglielmi et al., 2019; Shaldam et al., 2026). In a previous study by our group, a series of 2-aroylbenzo[*b*]thiophene analogues was designed, synthesized, and biologically evaluated, leading to the identification of compound 12 (hereafter referred to as BT12) as one of the most promising candidates (Arrighi et al., 2026). BT12 exhibited inhibitory activity toward both hMAO isoforms (IC_{50} = 0.062 ± 0.005 μM for hMAO-A and 0.045 ± 0.006 μM for hMAO-B) and demonstrated a modest neuroprotective effect in a 6-hydroxydopamine-induced SH-SY5Y cellular model, where it improved cell viability under oxidative stress conditions, supporting its potential as a lead compound (Arrighi et al., 2026). However, despite its promising biological profile, BT12 is characterized by extremely low aqueous solubility, which represents a major limitation for its pharmaceutical development, affecting formulation feasibility, bioavailability, and ultimately therapeutic efficacy.

In this scenario, drug delivery systems play a critical role not only in enabling the administration of poorly water-soluble compounds, but also in modulating their pharmacokinetic and release profiles (Eugster et al., 2025; Herdiana, 2025). In particular, controlled and sustained release systems may help to reduce fluctuations in drug concentration, limit off-target effects, and improve patient adherence (Eugster et al., 2024a). Lipid-based nanocarriers, and in particular liposomes, represent one of the most established platforms to address these challenges (Buttitta et al., 2025). Liposomes are versatile vesicular systems composed of one or more phospholipid bilayers surrounding an aqueous core, capable of incorporating both hydrophilic and lipophilic compounds (Akbarzadeh et al., 2013). Their clinical success, demonstrated by multiple approved formulations, highlights their ability to improve drug solubility, modulate pharmacokinetics, and reduce systemic toxicity. Nevertheless, the performance of liposomal systems is strongly influenced by lipid composition, which governs key membrane properties such as fluidity, permeability, and drug retention (Nsairat et al., 2022). Sphingomyelin, a major component of biological membranes, particularly in neuronal tissues, differs structurally from phosphatidylcholine due to the presence of an amide group capable of forming intermolecular hydrogen bonds (Fig. 1) (Ling et al., 2026). These interactions are associated with increased lipid packing and reduced membrane fluidity. In addition, sphingomyelin has been shown to interact more strongly with cholesterol, leading to enhanced membrane condensation and decreased permeability (Ramstedt and Slotte, 1999). Notably, sphingomyelin/cholesterol-based liposomal formulations have already been translated into clinical applications, as exemplified by the approved vincristine formulation Marqibo®, supporting the pharmaceutical relevance of this lipid system (Silverman and Deitcher, 2013).

From a technological perspective, microfluidic approaches have emerged as powerful tools for the reproducible and scalable production of lipid nanoparticles (Bonacorsi et al., 2025; Buttitta et al., 2024). By enabling controlled mixing at the microscale, microfluidics allows precise tuning of particle size and dispersity. When combined with systematic Design of Experiments (DoE) methodologies, this approach enables the systematic investigation of critical formulation and process parameters and their impact on key quality attributes (Eugster et al., 2024b).

Based on these considerations, this study aimed to develop and optimize lipid-based nanocarriers for the delivery of BT12 using a microfluidic approach supported by a DoE strategy. Two formulations were investigated: conventional hydrogenated soy phosphatidylcholine (HSPC)-based liposomes and sphingomyelin-based vesicles (sphingosomes), designed to exhibit comparable physicochemical characteristics while differing in membrane composition. A systematic DoE strategy was applied to evaluate the influence of formulation and process

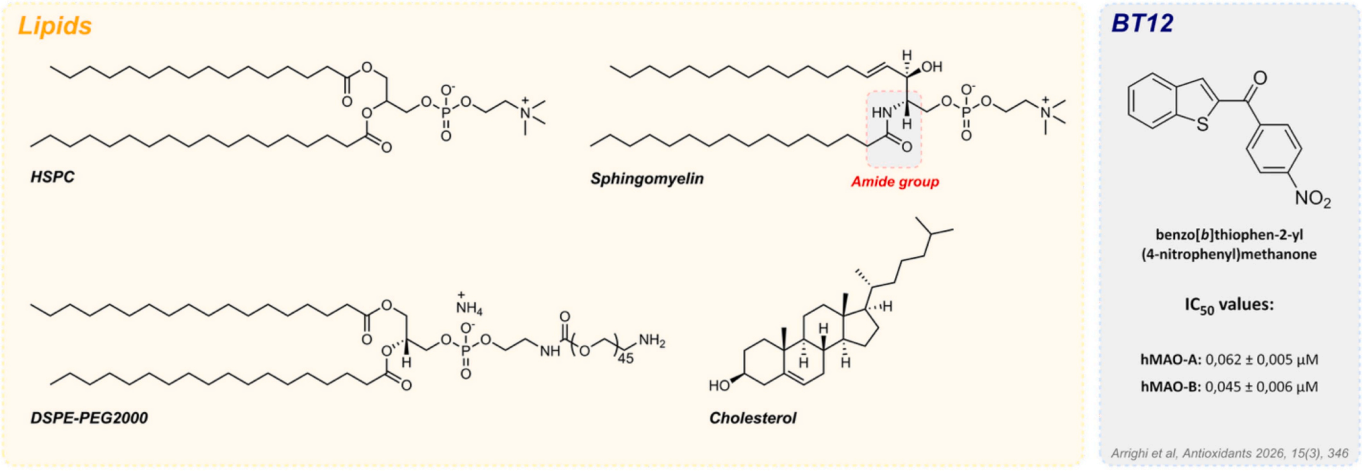

Fig. 1. Chemical structures of the lipid components used for nanoparticle formulation: HSPC, sphingomyelin, cholesterol, and DSPE-PEG2000 (lipid components, left) and of BT12 (benzo[b]thiophen-2-yl(4-nitrophenyl)methanone), the monoamine oxidase inhibitor synthesized by our group (right) (Arrighi et al., 2026).

variables on critical quality attributes, including particle size, PDI, and theoretical encapsulation efficiency (tEE%). By directly comparing these two lipid platforms under controlled conditions, this study seeks to elucidate the role of lipid composition in governing drug encapsulation and release behavior. In addition, the formulations were assessed from a biological perspective using SH-SY5Y neuronal-like cells to evaluate their cytocompatibility and cellular association and/or uptake. Through this integrated approach, the present work aims to support the rational design of lipid-based delivery systems for poorly water-soluble human monoamine oxidase inhibitors.

2. Materials and methods

2.1. Chemicals

Benzo[*b*]thiophen-2-yl(4-nitrophenyl)methanone (BT12) was synthesized by our research group via a previously optimized multistep synthetic route (Arrighi et al., 2026). Egg sphingomyelin (ESM), hydrogenated soy phosphatidylcholine (HSPC), and 1,2-distearoyl-*sn*-glycero-3-phosphoethanolamine-*N*-[methoxy(polyethylene glycol)-2000] (DSPE-PEG2000) were purchased from Lipoid (Ludwigshafen, Germany). Cholesterol (Chol) was obtained from Carbogen Amcis (Bubendorf, Switzerland). DiD dye (1,1′-Dioctadecyl-3,3,3′,3′-Tetramethylindodicarbocyanine, 4-Chlorobenzenesulfonate Salt) was purchased from Cayman Chemicals (Tallinn, Estonia). All other reagents, including HEPES, phosphate buffer components and organic solvents (HPLC grade), were purchased from Sigma-Aldrich (St. Louis, MO, USA). Human blood serum (HBS) was kindly provided by the Department of Clinical and Molecular Medicine, Sapienza University of Rome. Ultrapure water was obtained using a Milli-Q system (Millipore, France).

2.2. Microfluidic system setup

The microfluidic system used consisted of two Syringe Pumps NE-1010 (KF Technology, Italy) equipped with Inject Luer Lock syringes (B Braun, Germany), a tubing system and a microfluidic glass chip (Micromixer chip, cod. 3200401, Dolomite Microfluidics, UK). A 0.2 μm pore size Acrodisc syringe filter with 25 mm Supor EKV membrane (Pall, United States) was interposed between each pump and the tubing system, to prevent any clogging inside the glass chip. The organic pump was directly connected to the glass chip, while the aqueous pump was first connected to a T connector – 1/16″ (cod. 32008491, Dolomite Microfluidics, UK), to equally split the aqueous flow in two branches, before entering the glass chip (Fig. 2).

2.3. BT12 Quantification method

The quantification of BT12 was carried out using Shimadzu Prominence-i LC-2030C NT separation module equipped with a PDA detector. A Shimadzu Shim-pack GIST 5um; C18; 150 x 4.6 mm column was used. The column temperature was set at 30 ± 3 °C. The mobile phase consisted of (A) water with 0.01% (v/v) formic acid and (B) acetonitrile with 0.01% (v/v) formic acid. A gradient elution was applied at a flow rate of 1.0 mL/min over a total run time of 15 min. BT12 was detected at 318 nm, corresponding to its maximum absorbance in the UV spectrum. Quantification was performed using an external calibration curve in the range of 0.05–120 μg/mL. All measurements were carried out in triplicate, and results are expressed as mean ± standard deviation (Fig. 3).

2.4. Liposomes/sphingosomes preparation

Two primary lipids were evaluated for the production of the nanoparticles: HSPC, a widely utilized phosphocholine, and sphingomyelin, a chemically distinct sphingolipid. Depending on the selected membrane composition, lipid masses were accurately weighed together with the proper quantity of BT12 (according to the DoE parameters), dissolved in EtOH (≥99.8\% v/v) within a graduated flask, and stirred at 200 rpm for 10 min at room temperature until complete dissolution was visually confirmed. If undissolved particles were observed, additional stirring intervals of 5 min were applied until a clear solution was obtained. Liposomes/sphingosomes production via microfluidics was carried out by mixing the lipid solution with the aqueous phase under controlled experimental conditions using the previously described microfluidic system. Prior to each experiment, the system was primed to remove air bubbles and ensure stable flow conditions. Once steady-state conditions were achieved, formulations were collected for further characterization. For DiD labelled formulations, 0.1% DiD dye (molar ratio) was added into the lipid mixture and the same procedure was conducted to achieve a fluorescently labelled nanoparticle. All experimental condition tested are reported in the *Supplementary materials*.

2.5. Design of experiment

A DoE approach was employed to investigate the influence of microfluidic process parameters on nanoparticle critical quality attributes (CQAs), namely particle size, PDI, and tEE%. Experimental designs were generated using Minitab® 2018 software.

2.5.1. Screening DoE

A fractional factorial design (α = 0.05 a single; block and randomized runs) was used to identify critical process parameters (CPPs). In detail,

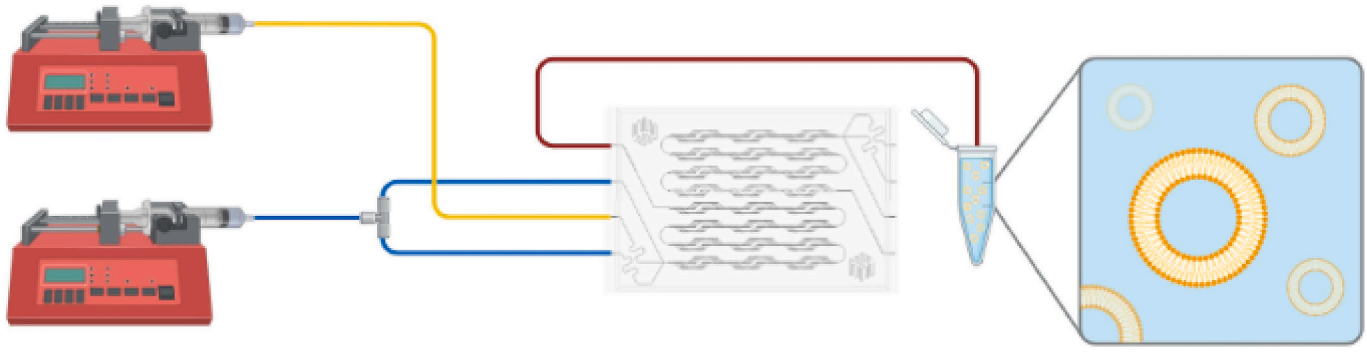

Fig. 2. Schematic representation of the microfluidic setup. The aqueous phase (blue line) is delivered to a T-connector, where the flow is equally split into two streams directed to the respective inlets of the micromixer chip. The organic phase (yellow line) is directly introduced into the chip. The micromixer chip is centrally positioned within the system, where nanoparticle formation occurs. The outlet channel (red line) is connected to a collection tube, allowing the direct recovery of the liposomal dispersion into an Eppendorf tube.

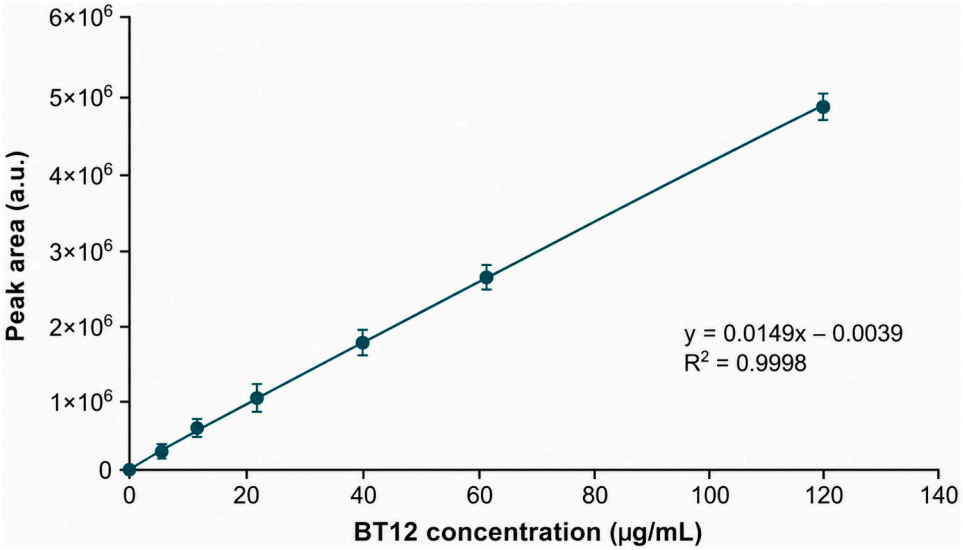

Fig. 3. Calibration curve of BT12 obtained by HPLC analysis at 318 nm.

two categorical and four continuous factors, with 2 experimental levels each, were selected for the investigation: aqueous medium (PBS; HEPES); drug to lipid ratio (D:L, 1:25; 1:75); Flow Rate Ratio between the aqueous and organic phase streams (FRR, 2.5–5.0); Total Flow Rate (TFR, 1.00–2.50 mL/min); cholesterol fraction into the overall lipid concentration (20–40 mol%) and DSPE-PEG2000 into the overall lipid concentration (5–10 mol%). A total of twenty-four experimental settings for each membrane were randomly generated by the software.

2.5.2. Full factorial DoE

Based on the screening results, a full factorial DoE ($\alpha = 0.05$) was performed to characterize the effects and interactions of the CPPs identified during the screening phase. Four of the six factors were fixed as default parameters (aqueous medium: PBS; D:L: 1:30; TFR: 2.50 mL/min; DSPE-PEG: 10 mol%), while FRR and cholesterol mol% were further investigated. A 2^2 full factorial design was employed, in which FRR and cholesterol content were evaluated at two levels each (FRR: 4 and 8; cholesterol: 30 and 50 mol%). A central point (FRR: 6; cholesterol: 40 mol%) was included to assess potential curvature effects. The resulting five experimental conditions were randomized and performed in triplicate for each formulation.

2.6. Theoretical encapsulation efficiency %

Purification of nanoparticles was performed using PD Mini-Trap Sephadex G-25 desalting columns (Cytiva, USA) to separate free BT12 from encapsulated drug. A 1 mL aliquot of freshly prepared formulations, containing theoretical BT12 amounts ranging from 10 to 80 μg depending on the experimental conditions, was loaded onto the column and eluted with PBS. The nanoparticle-containing fractions were collected, subjected to overnight lyophilization, and subsequently reconstituted in 1 mL of acetone. The samples were vortexed for 10 min, sonicated at 45 °C for 10 min, and centrifuged at maximum speed for 10 min to ensure complete extraction. An aliquot (0.5 mL) of the supernatant was collected and analysed through the HPLC. Since the calculation was based on the theoretical BT12 input rather than on the experimentally measured total BT12 amount, the encapsulation efficiency was defined as theoretical encapsulation efficiency (tEE%) and calculated according to the following equation:

$$tEE\% = \frac{BT12(purified)}{BT12(TOT)}.100\% \quad (1)$$

2.7. Determination of the physicochemical characteristics of the produced liposomal particles

The physicochemical characteristics of the nanoparticles, i.e. Z-average diameter, polydispersity and Zeta potential, were measured using a Litesizer700 (Anton Paar, Austria) with a 173° backscatter angle and a 658 nm helium–neon-laser. For size measurement, 100 μL of samples were diluted in 900 μL PBS buffer. After equilibrating the sample at 25 °C for 5 min, the measurement (20 runs × 10 s) was performed. The intensity size distribution of the sphingosomes/liposomes was typically unimodal; therefore, the autocorrelation function was analysed according to the cumulant method by the Kalliope™-software (Anton Paar). For Zeta potential measurements, 10 μL of samples were diluted in 990 μL of Milli-Q. The instrument was set at 200 V and 30 runs were performed. The Smoluchowski approximation with a Debye factor of 1.5 was used to calculate the mean zeta potential value.

2.8. Morphological and size distribution characterization using cryo-transmission electron microscopy

Morphology was also assessed using Cryo-Transmission Electron Microscopy (Cryo-TEM). Sample vitrification was carried out with a Mark IV Vitrobot (Thermo Fisher Scientific). For each sample, 3 μl of liposome solution, diluted with PBS to a final lipid concentration of 1.0 mg/mL, was applied to a Quantifoil R1.2/1.3 Cu 300-mesh grid previously glow-discharged at 30 mA for 30″ in a GloQube (Quorum Technologies). Immediately after the sample application, the grid was blotted in a chamber at 4 °C and 100% humidity and then plunge-frozen into liquid ethane. Vitrified grid was transferred to a Talos Arctica (Thermo Fisher Scientific) operated at 200 kV and equipped with a Ceta 16 M detector (Thermo Fisher Scientific). Images were acquired at a nominal magnification of 45,000x, corresponding to a pixel size of 2.3 Å/pixel with a defocus of −3.0 μm and with a total dose of 40 e-/Å2. The size distribution of the two formulations was determined from cryo-TEM images by measuring the diameter of at least 200 nanoparticles, with the open-source image processing software Fiji according to a 2-point identification method.

2.9. Short-term refrigerated storage stability of optimized products

Colloidal stability studies were conducted in accordance with ICH Q1A(R2) guidelines for short-term refrigerated storage (ICH Q1A(R2), 2003). Freshly prepared sphingosomes/liposomes were purified using

PD Mini-Trap Sephadex G-25 resin desalting column (see *supplementary materials* for experimental details). Nanoparticles were stored at 5 ± 3 °C at a total lipid concentration of 20 mM for up to 90 days. The physicochemical stability of the formulations was assessed over a period of 90 days by monitoring particle size and PDI. Measurements were performed by DLS at predefined time points (0, 1, 2, 3, 5, 7, 10, 15, 20, 30, 60, and 90 days).

2.10. Stability study in biologically relevant media

The colloidal stability of optimized liposomal and sphingosomal formulations in biologically relevant conditions was assessed following incubation in human blood serum (HBS). Purified nanoparticles were diluted in HBS to obtain final serum concentrations of 1% and 10% (v/v), maintaining a final lipid concentration of 20 mM. Samples were incubated at 37 °C, and changes in the mean hydrodynamic diameter were monitored over time (0, 1, 4, 8, 24, 48, 72, 120, and 168 h) using DLS. Control experiments were conducted under identical conditions in PBS.

2.11. In vitro release study of Bt12 from sphingosomes and liposomes

Optimized formulations were prepared and purified to achieve a final BT12 concentration of 10 μg/mL. A 1 mL aliquot of each formulation was loaded into dialysis membrane tubing (20 kDa MWCO, Spectrum Labs) and submerged in 19 mL of preheated PBS. The system was incubated at 37 °C under continuous magnetic stirring (150 rpm). Under these experimental conditions, sink conditions were maintained, since complete release of BT12 would result in a maximum theoretical concentration of approximately 0.5 μg/mL in the overall release system, which is well below the experimentally determined thermodynamic solubility of BT12 in PBS at 37 °C (8.43 ± 1.78 μg/mL; *Supplementary Materials*). At predetermined intervals (0, 0.5, 1, 2, 4, 8, 24, 48, and 72 h), 1 mL of the release medium was withdrawn and replaced with an equal volume of fresh preheated PBS. The collected samples were analyzed by HPLC to quantify BT12 release.

2.12. CELL culture

The human neuroblastoma cell line (SH-SY5Y) was purchased by ATCC (ATCC® No. CRL-2266) and cultured with Dulbecco's Modification of Eagle's Medium with 1 g/L glucose, L-glutamine, sodium pyruvate and 10% of Fetal Bovin Serum. Cells were maintained in an incubator at 37 °C with 5% CO_2 and 95% air. When cells reached 75–80% confluence, they were split to obtain subcultures (Guglielmi et al., 2025).

2.13. SAMPLE preparation for cell viability assay

Optimized liposomes and sphingosomes were prepared using a well-established formulation protocol. Following preparation, 2 samples of 4 mL each of liposomes and 2 samples of 3 mL each of sphingosomes were processed using Amicon® Ultra centrifugal filters (50 kDa molecular weight cutoff), employing two filter units per formulation.

Each sample was loaded into the respective Amicon units and centrifuged at 5000 × g for 30 min at 4 °C. After each of the first three centrifugation steps, DMEM was added to the filter units to restore volume. A fourth centrifugation was then performed without reconstituting the initial volume. Both formulations were subsequently characterized using DLS to assess their physicochemical properties and HPLC to quantify the internalized BT12. The concentrated BT12-loaded formulations were diluted with DMEM to achieve the desired final BT12 concentrations (12.5, 25, 50, 100, and 200 μM).

2.14. Cell viability

MTS assay (CellTiter 96® Aqueous One Solution Cell Proliferation Assay, Promega, Madison, WI, USA), was employed to assess the cell metabolic activity of SH-SY5Y cells. Specifically, 5×10^4 SH-SY5Y/well were seeded in a 96-multiwell plate and maintained in culture medium in an incubator for 24 h. SH-SY5Y cells were exposed to either empty nanoparticles (Liposomes-E and sphingosomes-E) as controls, or with BT12-loaded at concentrations of 12.5, 25, 50, and 100 μM and 200 μM for 24 h. Subsequently, 20 μL of MTS reagent was added to each well, and the plates were incubated at 37 °C for an additional 3 h. Cell metabolic activity, proportional to cell viability, was quantified by measuring absorbance at 490 nm using a Synergy™ HT multi-mode microplate reader (BioTek, Winooski, VT, USA) (De Colli et al., 2015; Marconi et al., 2019). To corroborate the data obtained from cell viability assay, parallel cultures were subjected to the trypan blue exclusion test at the identical 24-hour time point designated for the metabolic activity (MTS) assay. Following the incubation period, cell suspensions were thoroughly mixed with a 0.4% (w/v) trypan blue dye solution (Gibco, USA) at a 1:1 ratio. The mixture was immediately transferred to a Neubauer hemocytometer counting chamber. Cell enumeration was performed via brightfield light microscopy, where cells displaying prominent intracellular blue staining were classified as non-viable due to compromised membrane integrity, while clear, refractile cells were counted as viable.

2.15. Intracellular uptake

Confocal laser microscopy was used to study the cellular uptake of DiD-labeled liposomes and sphingosomes. SH-SY5Y cells were cultured in 8-well culture slides (Corning, Glendale, AZ, USA) at a density of 8,000 cells/well. At 24 h post-treatment, cells were fixed with 4% paraformaldehyde (PFA; BioOptica, Milan, Italy) in 0.1 M PBS (Lonza, Basel, Switzerland) for 1 h at room temperature. Following fixation, the cells were washed three times in PBS and permeabilized with 0.1% Triton X-100 (BioOptica) in PBS for 6 min. They were subsequently washed in PBS. The cells were then incubated for 1 h at 37 °C with Alexa Fluor 488 phalloidin green-fluorescent conjugate (1:400; A12379, Invitrogen) and DAPI (D3571, Invitrogen). Confocal fluorescence analysis was evaluated by image acquisition using a Zeiss LSM800 confocal system (Carl Zeiss, Jena, Germany) (Marconi et al., 2022). The quantification of DiD fluorescence was determined as arbitrary units of fluorescence per unit of cell surface area (Fluorescence A.U./μm^2) utilizing ImageJ software. Data were expressed as mean ± SD.

2.16. Statistics and reproducibility

All experiments were performed in triplicate unless otherwise specified. Data are presented as mean ± standard deviation. Statistical analyses, where applicable, are described within the corresponding sections of the Results and Discussion. No data points were excluded from the analysis. For cellular assays, statistical significance was established with GraphPad 5.01 (GraphPad, San Diego, CA, USA) software utilizing one-way ANOVA followed by post hoc Tukey's multiple comparisons analysis. Values of $p < 0.05$ were considered statistically significant.

3. Results and discussion

3.1. Rational design and doe optimization of bt12 loaded nanocarriers

This study aimed to develop and compare two lipid-based nanocarrier platforms for the delivery of BT12, a highly lipophilic hMAO inhibitor, using a rational design approach based on microfluidics and DoE. Two formulations were investigated: sphingomyelin-based vesicles (sphingosomes) and HSPC-based liposomes, chosen to enable a direct

comparison between a biomimetic lipid system and a conventional phosphatidylcholine-based platform. Both systems incorporated Chol to modulate membrane rigidity and permeability, along with DSPE-PEG2000 to provide steric stabilization, minimize opsonization, and extend systemic circulation (Roces et al., 2020). Notably, PEGylated nanoparticles have demonstrated enhanced blood–brain barrier (BBB) penetration, making them particularly suited for CNS-targeted therapies (Hu et al., 2019), further justifying their use in delivering BT12, an API with CNS-related therapeutic effects.

A DoE strategy was employed to systematically investigate and optimize CPPs affecting key CQAs, namely particle size, PDI, and tEE%. The optimization workflow consisted of three sequential steps: (i) Screening of CPPs, (ii) Full Factorial optimization, and (iii) Model-based refinement (Fig. 4).

3.1.1. Screening of CPPs

A screening DoE was performed to evaluate the influence of six formulation and process parameters, namely: buffer type, cholesterol content, DSPE-PEG2000 content, D:L, FRR, and TFR, on nanoparticle CQAs (Buttitta et al., 2024; Lou et al., 2019; Rebollo et al., 2022). For liposomal formulations, particle size ranged from 56 to 332 nm, with an average of 129 nm, while approximately 50% of formulations achieved a PDI below 0.2. Theoretical Encapsulation efficiency remained below 15% across all conditions, with values ranging from 5.1% to 14.6%. In contrast, sphingosomal formulations exhibited a broader variability in size, with several experimental conditions leading to unsuccessful nanoparticle formation (>1000 nm). Only a limited number of formulations achieved acceptable PDI values (≤0.2), and tEE% ranged from 1.2% to 21.5%, with an average of 8.3% (for further details see *Supplementary materials*). These results indicate that sphingomyelin-based systems are more sensitive to formulation parameters under non-optimized conditions. Moreover, the low tEE% observed across both formulations, aligned with the limitations of passive loading of lipophilic compounds within lipid bilayers (Roberts et al., 2022). Pareto analysis (Fig. 5) identified cholesterol content and FRR as the most influential CPPs across both systems. Cholesterol significantly affected all CQAs, highlighting its central role in modulating membrane organization and nanoparticle stability. FRR was particularly relevant for tEE%, confirming its importance in controlling solvent exchange kinetics and lipid self-assembly during microfluidic mixing(Roberts et al., 2022).

3.1.2. Full factorial optimization

Based on the screening results, cholesterol content and FRR were selected for further investigation, while other parameters were fixed to target nanoparticle CQAs (size < 100 nm; PDI ≈ 0.2; tEE%: maximized). A full factorial DoE was implemented, allowing for a comprehensive evaluation of the selected CPPs. In the tested conditions liposomes exhibited particle sizes between 69 and 124 nm, with a mean PDI of 0.215, while tEE% improved compared to the screening phase, reaching up to 33.1%. Sphingosomes displayed a narrower size distribution (71–86 nm) and lower PDI values, indicating improved homogeneity. Notably, tEE% was consistently higher (27.8–35.8%), suggesting enhanced drug retention within the sphingomyelin-based bilayer (see *Supplementary materials)*. Contour plots (Fig. 6) further illustrate the interaction between cholesterol content and FRR, defining the design space for optimized nanoparticle production. Interestingly, no statistically significant model could be established for sphingosomal size (Dean et al., 2017), indicating that size was largely independent of the investigated CPPs within the selected experimental range.

3.1.3. Model-based refinement

The screening and full factorial DoE phases enabled the development of predictive mathematical models describing the relationship between CPPs and nanoparticle CQAs. Overall, the generated models showed good predictive capability for particle size and encapsulation efficiency, with coefficients of determination (R^2) generally exceeding 70%, indicating a satisfactory fit between experimental and predicted data (Sedighi et al., 2019). In contrast, PDI models exhibited lower predictive performance, reflecting the intrinsic variability of this parameter and its sensitivity to multiple interdependent factors during nanoparticle formation (see Tables 1 and 2*)* (Lindsay et al., 2024).

Model-based optimization was used to identify optimal conditions for the two lipid systems. For HSPC-based liposomes, the optimal conditions corresponded to a cholesterol content of 44.75 mol% and a FRR of 8. For sphingosomes, optimal performance was achieved at a cholesterol content of 30 mol% and an FRR of 4. Wet-Lab validation confirmed the robustness and reliability of the developed models. As summarized in Tables 3 and 4, the optimized liposomal formulation exhibited a particle size of 86 ± 6 nm, a PDI of 0.222 ± 0.046, and a theoretical encapsulation efficiency of 20.4 ± 0.7%, in good agreement with predicted values. Similarly, sphingosomes showed a particle size of 78 ± 5 nm, a PDI of 0.178 ± 0.044, and a tEE% of 35.8 ± 1.1%, closely matching model predictions. It is worth noting that the theoretical encapsulation efficiencies obtained for both systems can be considered moderate, even when accounting for the intrinsic limitations of passive loading for highly lipophilic and non-ionizable compounds such as BT12 (Roberts et al., 2022). In this context, drug incorporation is primarily governed by partitioning within the lipid bilayer, which inherently limits the achievable loading capacity. However, in the present study, theoretical encapsulation efficiency was not maximized as an isolated parameter, but rather optimized together with other CQAs (particle size and PDI). This strategy was essential to obtain well-defined and reproducible nanosystems, enabling a direct and controlled comparison between liposomes and sphingosomes. Consequently, the reported tEE% values reflect a balance between maximizing drug loading and preserving the physicochemical properties required for nanoparticle

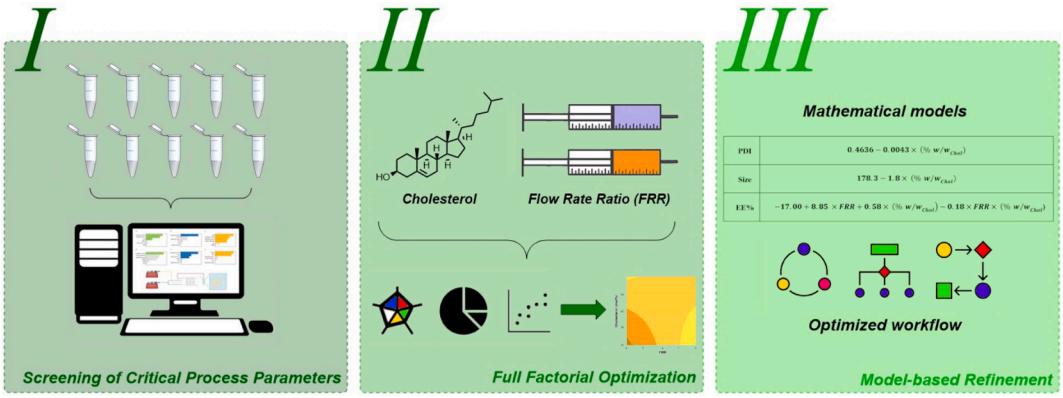

Fig. 4. Optimization workflow of BT12-loaded nanocarriers: (i) screening of CPPs, (ii) full factorial optimization, and (iii) model-based refinement.

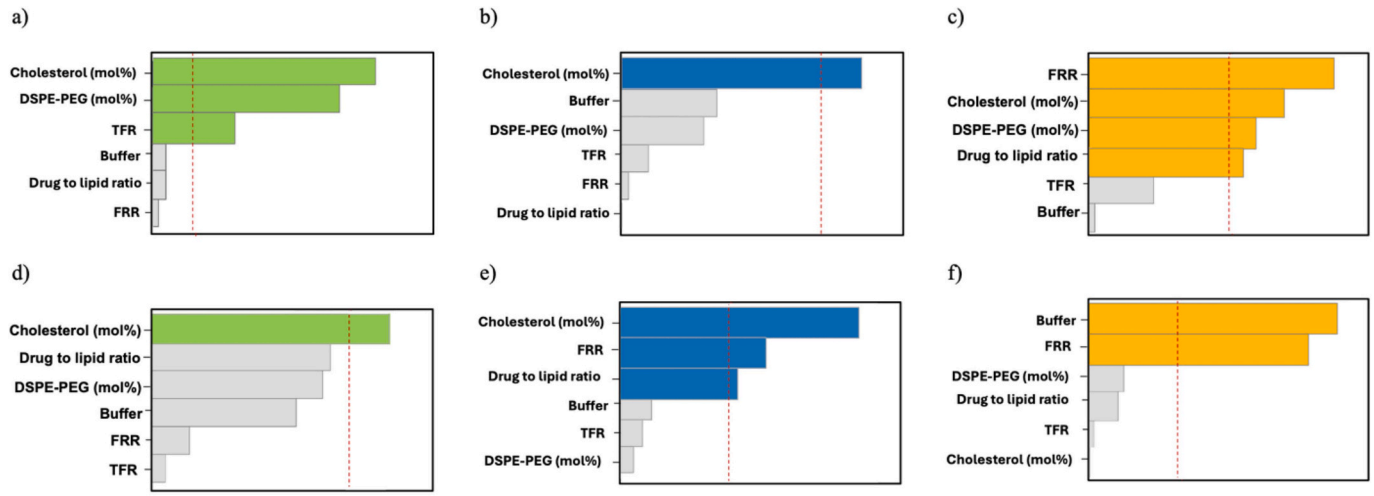

Fig. 5. Pareto charts depicting the size, PDI, and tEE% from the screening DoE of critical process parameters. Figures a), b), and c) correspond to the size, PDI, and tEE% of liposomal formulations, respectively. Figures d), e), and f) represent the size, PDI, and tEE% of sphingosomes. The red line indicates the threshold effect size at a 0.05 significance level. Factors represented by bars extending beyond the red line have a significant impact on the evaluated parameter, while factors with bars shorter than the red line are considered non-significant.

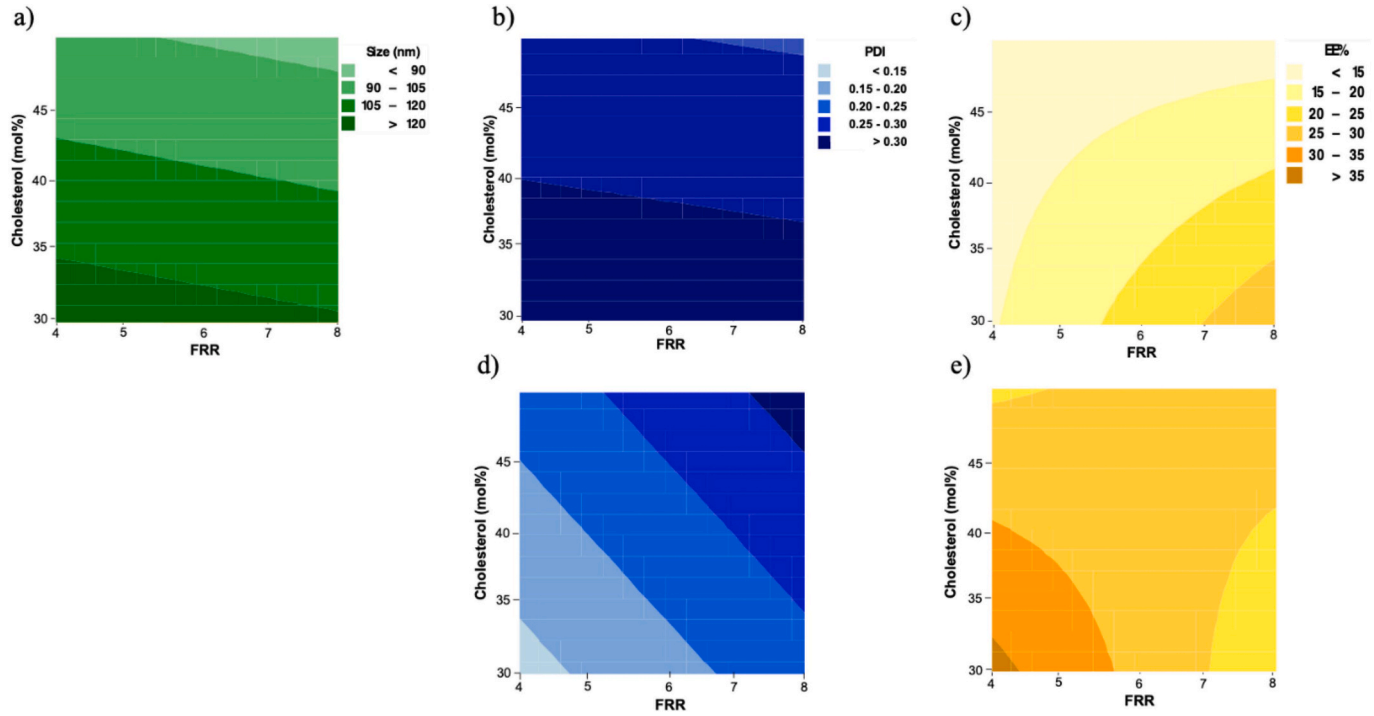

Fig. 6. Contour plots obtained from the full factorial DoE study. Figures a), b), and c) show the effect of Chol (mol%) and FRR on size (green), PDI (blue) and tEE% (orange) in liposomes. While Figures d), and e) show results for PDI (blue) and tEE% (orange) for the sphingosomal membrane, respectively.

Table 1
Summary of regression analysis of models for liposomes from characterization full factorial DoE.

HSPC liposomes	Model Equations including important factors in uncoded units	R^2	Predicted R^2
PDI	$0.4636 - 0.0043 \times (\%w/w_{Chol})$	62.95%	52.55%
Size	$178.3 - 1.8 \times (\%w/w_{Chol})$	79.20%	72.87%
tEE%	$-17.00 + 8.85 \times FRR + 0.58 \times (\%w/w_{Chol}) - 0.18 \times FRR \times (\%w/w_{Chol})$	81.28%	58.32%

comparability. These findings underline the importance of adopting a holistic formulation approach, in which theoretical encapsulation efficiency is inherently constrained by the need to maintain overall nanoparticle performance, particularly for highly lipophilic compounds such as BT12. These findings suggest that, under controlled formulation conditions, lipid composition plays a key role in governing drug retention within the bilayer, with sphingomyelin-based systems providing enhanced encapsulation of BT12.

Table 2
Summary of regression analysis of models for sphingosomes from characterization full factorial DoE.

Sphingosomes	Model Equations including important factors in uncoded units	R^2	Predicted R^2
PDI	$-0.109 + 0.025 \times FRR + 0.005 \times (\%w/w_{Chol})$	53.35%	33.31%
tEE%	$97.70 - 10.70 \times FRR - 1.53 \times (\%w/w_{Chol}) + 0.23 \times FRR \times (\%w/w_{Chol})$	73.71%	31.98%

Table 3
Model-based optimization results and experimental validation for HSPC liposomes.

HSPC liposomes	Required condition	Predicted value	Experimental value
PDI	Minimize	0.266	0.222 ± 0.046
Size (nm)	<100	96	86 ± 6
tEE%	Maximize	16.8%	20.4 ± 0.7

Table 4
Model-based optimization results and experimental validation for sphingosomes.

Sphingosomes	Required condition	Predicted value	Experimental value
PDI	Minimize	0.129	0.178 ± 0.044
Size (nm)	<100	/	78 ± 5
tEE%	Maximize	36.6%	35.8 ± 1.1

3.2. Morphology and surface charge analysis

The morphology of the optimized formulations was investigated by Cryo-TEM, while surface charge was assessed by zeta potential measurements to evaluate colloidal stability. The integration of Cryo-TEM and zeta potential data facilitates a comprehensive evaluation of nanosystems, bridging structural characterization with colloidal stability assessment (Kuntsche et al., 2011; Lee et al., 2022; Wibroe et al., 2016). Cryo-TEM analysis (Fig. 7**a,b,d and e**) revealed that both liposomes and sphingosomes exhibited well-defined spherical unilamellar vesicles, with clearly distinguishable aqueous cores. Minor background artifacts, manifested as dark black dots, were attributable to residual ethane impurities from cryo-plunging procedures, a well-documented phenomenon in vitrification protocols (Grassucci et al., 2007). Cryo-TEM-derived diameters (76 ± 53 nm for liposomes and 82 ± 50 nm for sphingosomes) were consistent with hydrodynamic sizes obtained by DLS, confirming the absence of significant aggregation (Fig. 7c and f). Zeta potential values were close to neutrality (−1.9 ± 3.0 mV for liposomes and −0.5 ± 1.2 mV for sphingosomes), which would typically suggest limited electrostatic stabilization. However, no evidence of aggregation or structural instability was observed in Cryo-TEM images. This apparent discrepancy can be explained by the presence of DSPE-PEG2000, which provides steric stabilization through the formation of a hydrated polymer corona at the nanoparticle surface. Under these conditions, steric repulsion dominates over electrostatic interactions, ensuring colloidal stability despite near-neutral surface charge (Giakoumatos et al., 2022; Thevenot et al., 2007). Overall, these results confirm that both formulations exhibit comparable nanoscale dimensions and structural integrity, enabling a direct comparison of their performance as a function of lipid composition.

3.3. Stability assessment

Following physicochemical optimization, the colloidal stability of the selected formulations was evaluated. In this context, stability was investigated in terms of nanoparticle dispersion behavior, by monitoring particle size and polydispersity index under both refrigerated storage conditions and in biologically relevant media. These parameters represent key indicators of nanoparticle integrity and are widely used in

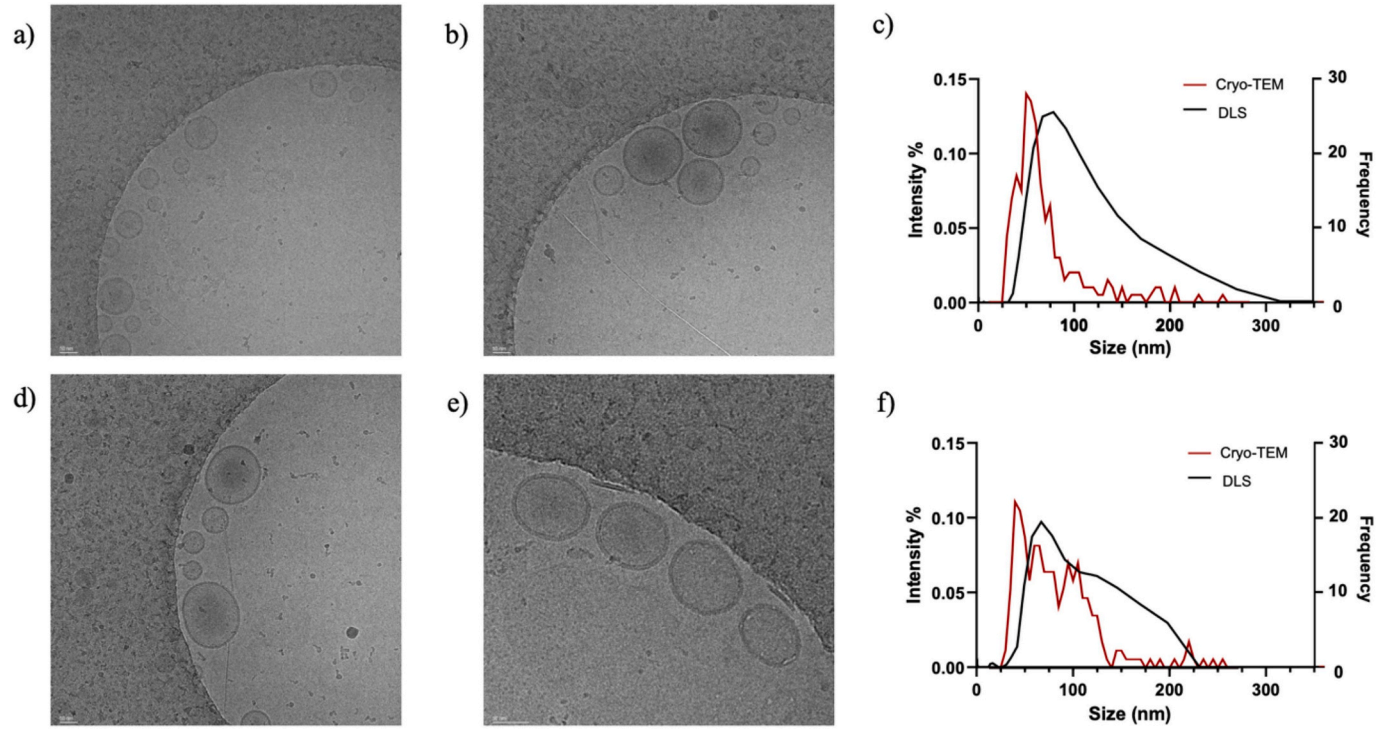

Fig. 7. Cryo-TEM images of optimized liposomes (a,b) and sphingosomes (d,e). Scale bars: 50 nm. Size distributions obtained from Cryo-TEM analysis (red) are overlaid with DLS intensity-weighted hydrodynamic diameter distributions (black) for liposomes (c) and sphingosomes (f). Cryo-TEM size distributions were determined by manual analysis of ≥ 200 nanoparticles using Fiji software.

early-stage formulation development, enabling a controlled comparison of the influence of lipid composition on nanosystem behavior.

3.3.1. Short-term refrigerated storage stability of optimized products in PBS (pH 7.4)

Colloidal stability under refrigerated conditions (5 ± 3 °C) in phosphate-buffered saline (PBS, pH 7.4) is a key requirement for the practical use of lipid-based formulations. Both liposomes and sphingosomes demonstrated good physicochemical stability over the evaluation period, maintaining nanoscale size and narrow size distribution (Fig. 8) up to 90 days. HSPC liposomes exhibited a slight initial decrease in size from 92 ± 2 nm (Day 0) to 80 ± 1 nm (Day 3), followed by stabilization, with a final diameter of 83 ± 4 nm at Day 90. Similarly, PDI values decreased from 0.22 ± 0.01 to approximately 0.20, indicating improved homogeneity after initial equilibration. Sphingosomes showed a comparable trend, with an initial size reduction from 75 ± 2 nm to 69 ± 1 nm (Day 3), followed by stable values up to Day 15 and a moderate increase to 83 ± 1 nm at Day 90. PDI values remained within an acceptable range throughout the study, with only minor variations over time. Overall, both formulations preserved their colloidal stability under refrigerated conditions, with no evidence of aggregation or significant destabilization.

3.3.2. Stability study in biologically relevant media

Since the developed formulations are intended for systemic administration, their colloidal stability under biologically relevant conditions was evaluated by monitoring particle size upon incubation in human serum. The interaction of lipid-based nanocarriers with biological fluids is a critical factor influencing their in vivo performance, as protein adsorption may affect colloidal stability and circulation behavior (Nele et al., 2024). For both formulations, a time-dependent increase in particle size was observed under all tested conditions. Interestingly, the most pronounced size increase occurred in PBS, where liposomes reached 133 ± 10 nm (+44%) and sphingosomes 112 ± 6 nm (+36%). In contrast, the presence of serum mitigated this effect, resulting in a more moderate and consistent size increase. Liposomes reached final diameters of 127 ± 10 nm (+42%) and 112 ± 12 nm (+22%) in 1% and 10% serum, respectively, while sphingosomes increased to 100 ± 4 nm (+19%) and 89 ± 6 nm (+21%) under the same conditions (Fig. 9). The reduced size increase observed in serum-containing media suggests a stabilizing effect on nanoparticle dispersion, potentially associated with protein adsorption at the nanoparticle surface. However, the underlying mechanisms cannot be conclusively determined based on DLS measurements alone. In this context, we hypothesize a potential stabilizing effect related to serum proteins that may act as dynamic stabilizing agents, reducing vesicle fusion or restructuring phenomena that are more pronounced in buffer alone (Monopoli et al., 2012). Notably, sphingosomes exhibited a more limited size variation already at low serum concentration (1%), whereas liposomes required higher serum content (10%) to achieve a comparable effect. This behavior may reflect differences in nanoparticle-protein interactions as a function of lipid composition. In this regard, previous studies have reported that sphingomyelin- and phosphatidylcholine-based nanocarriers can exhibit distinct protein adsorption patterns, which may influence their physicochemical behavior in biological environments (Ling et al., 2026). Overall, these findings indicate that both formulations maintain colloidal stability under physiologically relevant conditions, as reflected by the absence of marked aggregation phenomena and the relatively controlled increase in particle size over time.

3.4. In vitro release study of Bt12 from sphingosomes and liposomes

The in vitro release kinetics of free BT12 and optimized formulations were evaluated in PBS (pH 7.4) at 37 ± 1 °C using the dialysis bag method. Free BT12 exhibited, as expected, a rapid and complete release, characterized by an initial burst due to its fast diffusion across the dialysis membrane, with 38 ± 9% released within the first 4 h and 86 ± 19% after 8 h, followed by a plateau at 24 h. In contrast, both optimized formulations showed a controlled and sustained release. HSPC liposomes released 14 ± 2% after 4 h and 33 ± 2% at 8 h, achieving complete release at approximately 48 h, while sphingosomes exhibited a slower release profile, with 13 ± 2% released at 8 h and an incomplete release even at 72 h (52 ± 8%) (Fig. 10).

These findings underscore the critical role of lipid composition in modulating drug release, despite the formulations exhibiting comparable physicochemical characteristics (Pamunuwa et al., 2016). The slower release observed for sphingosomes may be tentatively attributed to the intrinsic structural properties of sphingomyelin-based membranes. Indeed, previous studies have shown that sphingomyelin can form more ordered and tightly packed bilayers compared to phosphatidylcholine systems, due to the presence of an amide group enabling intermolecular hydrogen bonding and reduced lipid mobility (Niemelä et al., 2004). In addition, sphingomyelin has been reported to interact more strongly with cholesterol than phosphatidylcholine, leading to

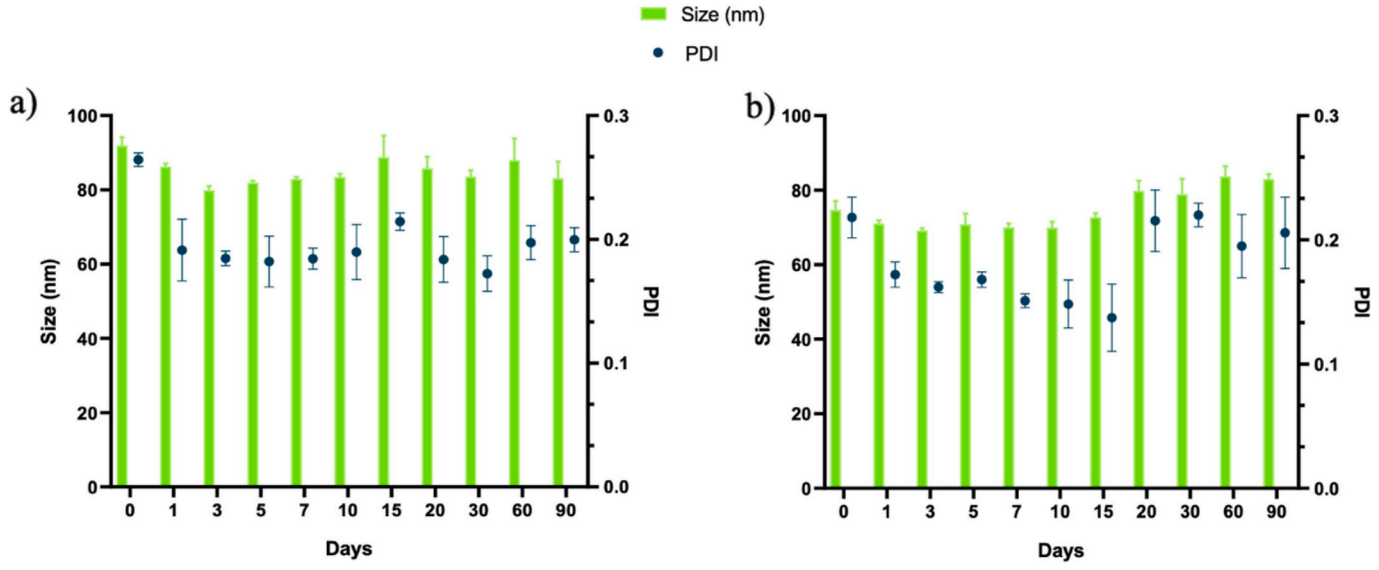

Fig. 8. Short-term colloidal stability of liposomes (a) and sphingosomes (b) was evaluated at 5 ± 3 °C. Nanoparticles size (green columns) and polydispersity index (blue dots) were monitored over time. Data are presented as mean ± standard deviation.

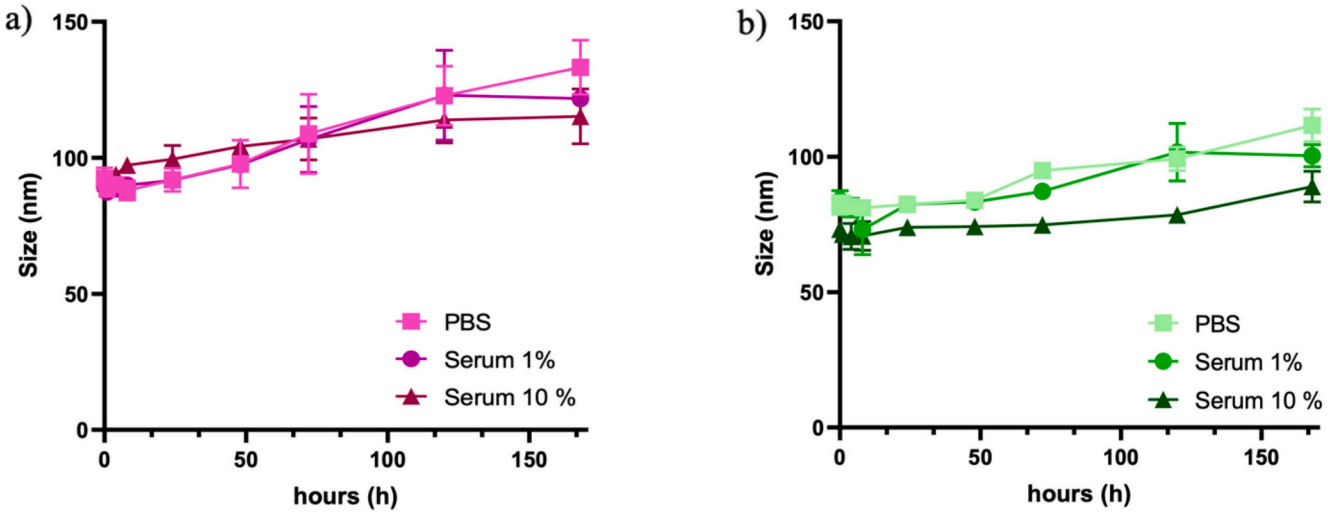

Fig. 9. Colloidal stability in biorelevant media at 37 ± 1 °C of liposomes (a) and sphingosomes (b) formulations. Data are presented as mean ± standard deviation.

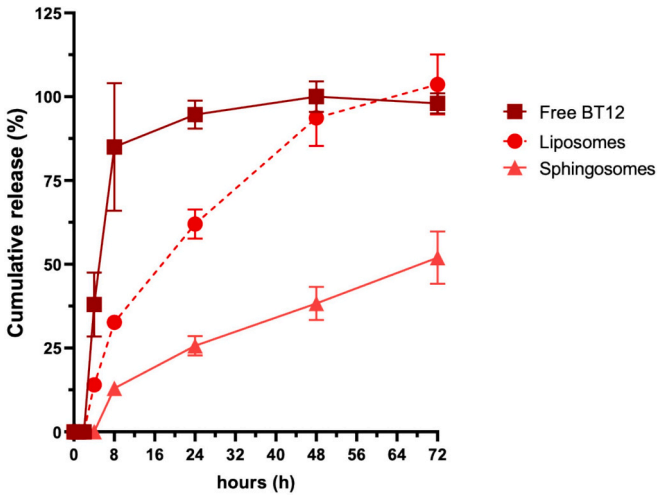

Fig. 10. In vitro release profiles of BT12 in PBS at 37 ± 1 °C comparing free drug with liposomal and sphingosomal formulations. Data are presented as mean ± standard deviation..

increased membrane condensation and decreased permeability (Ramstedt and Slotte, 1999). In this context, it is reasonable to hypothesize that such features may contribute to a reduced diffusion of BT12 across the bilayer, resulting in a more sustained release profile. The absence of a pronounced burst release in both systems suggests that BT12 is effectively associated with the lipid bilayer rather than loosely adsorbed or surface-associated, supporting a diffusion-controlled release mechanism. This behavior may help reduce the risk of acute toxicity while promoting prolonged drug exposure. Overall, the controlled release profiles observed for both formulations, and particularly for sphingosomes, could be advantageous in improving therapeutic efficacy and reducing dosing frequency (Rahnfeld and Luciani, 2020).

3.5. Cellular studies

With the aim of biologically characterizing the two developed formulations, cell viability and association and/or uptake were investigated to assess their suitability as drug delivery systems. While the evaluation of cell viability is essential to determine the safety profile of the formulations, efficient internalization of the nanosystem is required to ensure biological activity. Indeed, hMAO are flavoenzymes localized on the outer mitochondrial membrane; therefore, drug efficacy critically depends on the ability of the compounds to cross the cell membrane and reach their intracellular target.

3.5.1. Sample preparation for cell viability assay

To achieve the highest possible BT12 level while preserving the physicochemical properties of the nanosystems, the optimized formulations were concentrated as described in Section 2.13. This procedure yielded concentrated BT12-loaded liposomes and sphingosomes with the characteristics reported in Table 5.

Based on the BT12 levels measured in the concentrated formulations, appropriate dilutions were prepared in DMEM to obtain the final drug amounts used in the cell viability experiments. The corresponding lipid doses administered to the cells are reported in Table 6.

3.5.2. Cell viability

The effects of liposomes and sphingosomes on cell viability were evaluated using the MTS assay, a colorimetric method widely employed to assess cell viability, proliferation, and cytotoxicity in cultured cells. This cell line was chosen for two main reasons: (i) it has previously been employed for the biological characterization of free BT12 (Arrighi et al., 2026), enabling direct comparison with earlier findings; and (ii) SH-SY5Y is widely used as an in vitro neuronal-like model, making it suitable for evaluating how differences in formulation composition influence cellular interaction in a CNS-relevant system. The MTS assay was performed after 24 h of incubation to evaluate cell viability following treatment with free BT12 at concentrations of 12.5, 25, 50, and 100 μM, empty formulations used as controls (Lipo-E and Sph-E), and BT12-loaded liposomes or sphingosomes at drug concentrations of 12.5, 25, 50, 100, and 200 μM (Fig. 11). As reported in Table 6, these formulations also differed in their lipid content. Indeed, the concentrated loaded formulations were subjected to successive dilutions to achieve the desired BT12 levels, thereby also modifying the lipid amount

Table 5
Results of the concentration/diafiltration study performed on the optimized BT12-loaded nanosystems.

Formulations	Size	PDI	Lipid concentration (mM)	HPLC BT12 concentration (μM)
Lipo Empty	39.7	0.192	10.74	
Lipo Loaded	49.5	0.185	24.70	375
Sph Empty	37.7	0.205	11.44	
Sph Loaded	46.9	0.194	26.10	703

Table 6
Final BT12 and lipid concentrations used for cell treatment after dilution of the concentrated BT12-loaded formulations in DMEM.

Formulations	Lipid concentration (mM)	BT12 concentration (μM)
Lipo-E	10.74	
Lipo BT12 – 12.5 μM	0.82	12.5
Lipo BT12 – 25 μM	1.65	25
Lipo BT12 – 50 μM	3.30	50
Lipo BT12 – 100 μM	6.59	100
Lipo BT12 – 200 μM	13.17	200
Sph-E	11.44	
Sph BT12 – 12.5 μM	0.46	12.5
Sph BT12 – 25 μM	0.93	25
Sph BT12 – 50 μM	1.86	50
Sph BT12 – 100 μM	3.71	100
Sph BT12 – 200 μM	7.43	200

administered in the different samples. Free BT12 and both empty formulations were generally well tolerated by SH-SY5Y cells. Although empty liposomes showed a slightly higher mean viability than empty sphingosomes, this difference was not statistically significant and should therefore be interpreted only as a trend. Among the BT12-loaded systems, liposomes displayed a more favourable cytocompatibility profile than sphingosomes, particularly at higher drug concentrations. In particular, BT12-loaded sphingosomes induced a statistically significant reduction in cell viability from 25 μM onward. This effect is unlikely to be explained solely by lipid content, as the lipid amount administered with BT12-loaded sphingosomes was consistently lower than that of the corresponding empty formulations. Rather, it may reflect the association of increasing BT12 levels with the sphingosome system. At the highest tested concentration, 200 μM, BT12-loaded sphingosomes showed significantly lower cell viability compared with the corresponding BT12-loaded liposomes, supporting the better tolerability of the liposomal formulation under the investigated experimental conditions. Notably, both nanocarrier systems enabled cellular exposure to BT12 at 200 μM, a concentration that could not be achieved with the free compound because of its limited solubility.

To corroborate the MTS findings using a direct cell-counting approach, a parallel Trypan blue exclusion assay was performed at the same 24 h time point. The dye exclusion assay showed a trend consistent with the metabolic activity profiles, supporting the overall cytocompatibility results obtained by MTS assay (Fig. 11, B and C). Bright-field microscopy revealed a predominance of clear, refractile viable cells and only a low number of Trypan blue-positive non-viable cells in both empty formulations. Quantification of viable and dead cells further confirmed the absence of marked membrane damage under most experimental conditions, while supporting the more favourable cytocompatibility profile of BT12-loaded liposomes compared with BT12-loaded sphingosomes at higher concentrations.

3.5.3. *Cell association and/or uptake of optimized nanoparticles*

Cellular uptake of liposomes and sphingosomes was evaluated using confocal microscopy following labeling with the lipophilic fluorescent dye DiD (Roveri et al., 2017). To further characterize nanoparticle–cell interactions, Alexa Fluor 488 phalloidin and DAPI were employed to stain the actin cytoskeleton and nuclei, respectively. Confocal imaging revealed a clear intracellular distribution of DiD fluorescence (red) within the cytoplasmic region, delineated by actin filaments (green) and

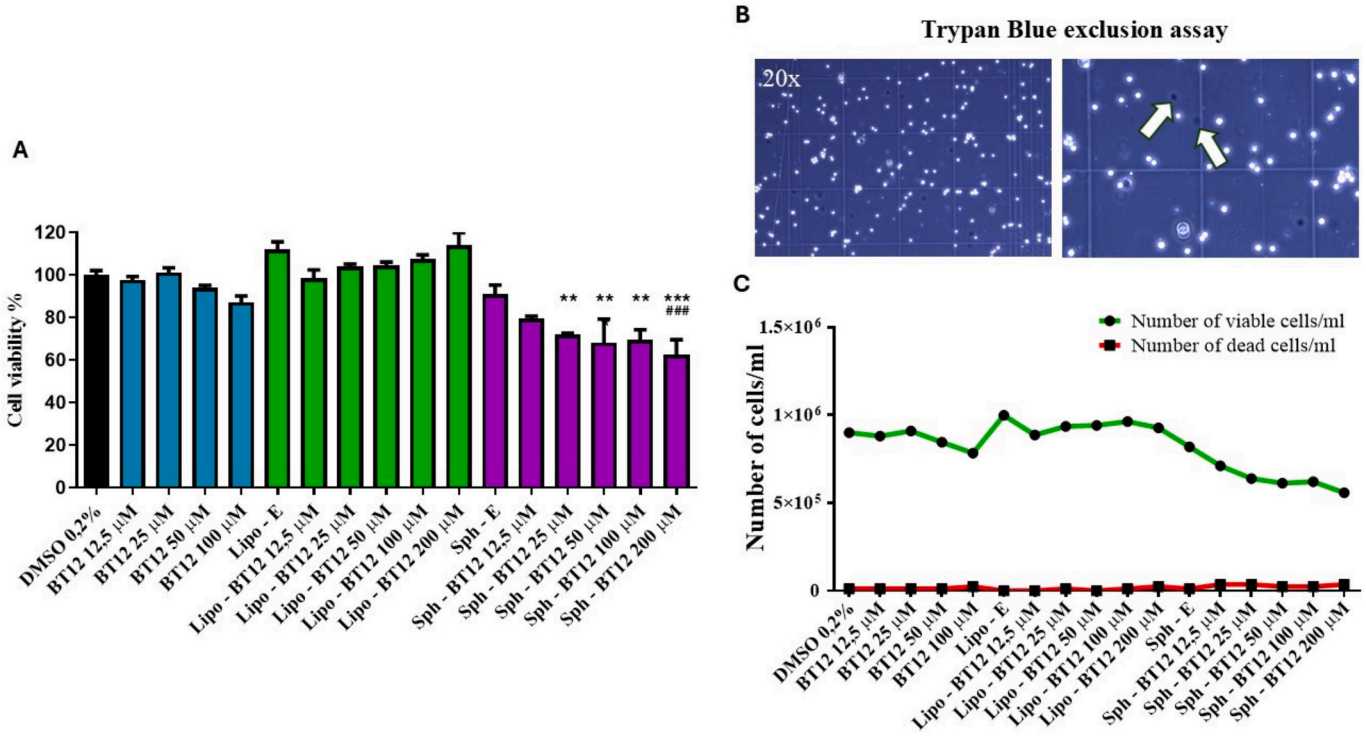

Fig. 11. A) Cell viability was assessed by MTS assay and normalized to vehicle-treated control cells, corresponding to SH-SY5Y cells treated with DMSO 0.2% final concentration. The bar graph shows the viability of SH-SY5Y cells exposed for 24 h to free BT12 at 12.5, 25, 50, and 100 μM; empty liposomes (Lipo-E) and empty sphingosomes (Sph-E); BT12-loaded liposomes or sphingosomes at drug concentrations of 12.5, 25, 50, 100, and 200 μM. Data are reported as mean ± SD. Statistical analysis was performed by one-way ANOVA followed by Tukey's multiple comparisons test. **$p < 0.01$ and ***$p < 0.001$ vs vehicle-treated control cells (DMSO 0.2%). ###$p < 0.001$ indicates the comparison between Sph-BT12 200 μM and the corresponding Lipo-BT12 200 μM formulation. B) Representative bright-field microscopy images of a single-cell suspension stained with 0.4% Trypan blue. Viable cells maintained membrane integrity, excluded the dye, and appeared clear and refractile, whereas non-viable cells, indicated by white arrowheads, showed Trypan blue uptake due to compromised membrane integrity. Images were acquired using a standard hemocytometer grid at 20 × magnification. C) Quantification of viable and dead cells across the experimental conditions, expressed as number of cells/mL. The green line represents viable cells, identified by Trypan blue exclusion, whereas the red line represents dead cells, identified by Trypan blue uptake.

surrounding the nuclei (blue), confirming effective association and/or uptake of both liposomes and sphingosomes in SH-SY5Y cells after 24 h of incubation (Fig. 12).

Quantitative analysis of DiD-associated fluorescence revealed significantly higher fluorescence intensity in cells treated with both sphingosomes and liposomes compared with the control (CTRL) group (Fig. 13), indicating enhanced nanocarrier–cell association and/or uptake. However, no statistically significant difference was observed between the two formulations under the investigated experimental conditions, although liposomes showed a slightly higher mean fluorescence intensity than sphingosomes.

This comparable behavior may be attributed, at least in part, to the similar physicochemical characteristics of the nanoparticles, particularly their size, surface charge, and PEGylation profile, which may partially mask differences arising from lipid composition(He et al., 2010; Suk et al., 2016).

4. Conclusions

This study presents a formulation-driven, comparative evaluation of lipid-based nanocarriers for the delivery of BT12, a poorly water-soluble hMAO inhibitor previously identified in a medicinal chemistry study, using a microfluidic approach combined with a Design of Experiments strategy. HSPC-based liposomes and sphingosomes were engineered to exhibit comparable physicochemical properties, enabling a controlled evaluation of the impact of lipid composition on nanocarrier performance. While both formulations showed similar size, dispersity, and stability in physiologically relevant conditions, lipid composition significantly influenced drug encapsulation and release behavior. In particular, sphingosomes exhibited a comparatively higher tEE% than HSPC liposomes, although the absolute values remained moderate, and a more sustained release profile, consistent with the reduced permeability of sphingomyelin-based bilayers. Biological evaluation in SH-SY5Y cells confirmed efficient association and/or uptake of both systems, with no evident differences between formulations, suggesting that cellular uptake is primarily governed by surface characteristics such as size and PEGylation. In contrast, cytocompatibility was influenced by lipid composition, with sphingosomes showing a moderate reduction in cell viability compared to HSPC-based liposomes, also observed for empty formulations, indicating a membrane-driven effect. Overall, these findings highlight that distinct formulation parameters govern different aspects of nanocarrier performance, with lipid composition primarily affecting drug retention and biological response, and surface properties playing a dominant role in cellular association and/or uptake. This work provides a rational framework for the design of lipid-based delivery systems and supports their application for improving the delivery of promising but poorly water-soluble hMAO inhibitors.

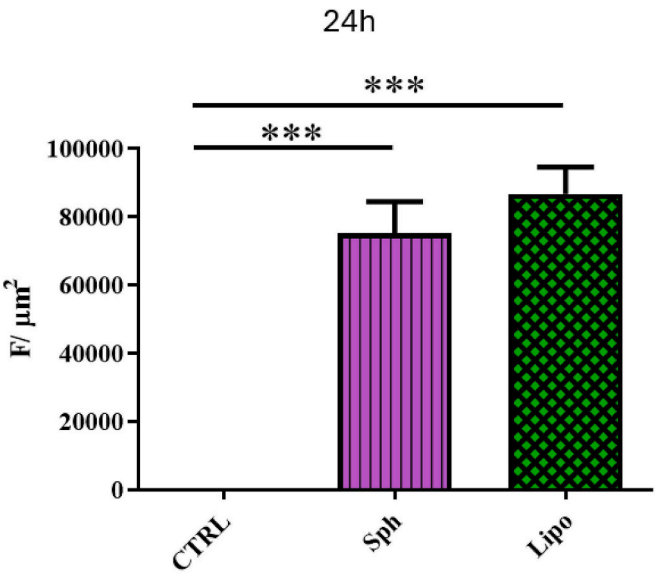

Fig. 13. The histogram displays the quantitative analysis of DiD fluorescence intensity performed using ImageJ software in CTRL, sphingosome-, and liposome-treated samples. ***p < 0.001 vs vehicle-treated control cells (DMSO 0.2%).

CRediT authorship contribution statement

Giorgio Buttitta: Writing – original draft, Visualization, Validation, Methodology, Investigation, Formal analysis, Conceptualization. **Michele Coluccia:** Writing – review & editing, Visualization. **Simone Bonacorsi:** Writing – review & editing. **Francesca Diomede:**

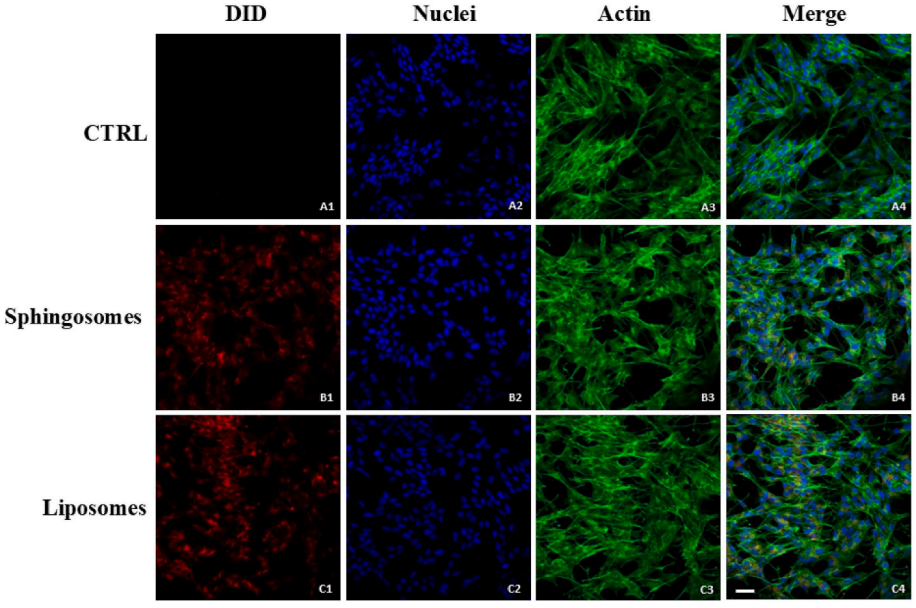

Fig. 12. Confocal microscopy images of SH-SY5Y cells show the uptake of DiD-labeled liposomes and sphingosomes (red) after 24 h of incubation. The images display DiD-labeled membranes (red), actin filaments (green), and nuclei (blue) at a scale bar of 20 µm.

Investigation, Funding acquisition. **Guya Diletta Marconi:** Writing – original draft, Investigation, Conceptualization. **Jacopo Pizzicannella:** Writing – review & editing. **Elena De Falco:** Writing – review & editing, Funding acquisition. **Paolo Guglielmi:** Writing – original draft, Visualization, Project administration, Funding acquisition, Formal analysis, Conceptualization.

Funding

This research was funded by the European Union—Next Generation EU — 2022HXMY4P—CUP D53D23010340006 Research Project By Relevant National Interest (PRIN 2022), Unity is strength: a novel tool based on human MonoAmine Oxidase B Inhibitors and MEsenchymal Stem Cells Se-cretome. Novel insights into the molecular Ular mechanisms of ParkiNson's (MAOBI-MESCS-UNION).

Declaration of competing interest

The authors declare that they have no known competing financial interests or personal relationships that could have appeared to influence the work reported in this paper.

Acknowledgments

Michele Coluccia was supported by Fondazione Umberto Veronesi. Special thanks to Luigia Fonticoli for performing the MTS assay.

Appendix A. Supplementary data

Solubility determination of BT12 in different experimental conditions; BT12 purification method; experimental conditions of the different DoEs and associated results. Supplementary data to this article can be found online at https://doi.org/10.1016/j.ijpharm.2026.127207.

Data availability

No data was used for the research described in the article.

References

Akbarzadeh, A., Rezaei-Sadabady, R., Davaran, S., Joo, S.W., Zarghami, N., Hanifehpour, Y., Samiei, M., Kouhi, M., Nejati-Koshki, K., 2013. Liposome: Classification, preparation, and applications. Nanoscale Res. Lett. 8. https://doi.org/10.1186/1556-276X-8-102.

Arrighi, F., Berrino, E., Guglielmi, P., Carradori, S., Marconi, G.D., Pizzicannella, J., Guarnieri, S., Tuccinardi, T., Poli, G., Pepi, F., Troiani, A., Salvitti, C., Di Noi, A., Coluccia, M., Buttitta, G., Pontecorvi, V., Granese, A., Chimenti, P., Secci, D., Petzer, A., Petzer, J.P., Diomede, F., 2026. Novel insights on benzo[b]thiophene analogues for MAO-B inhibition and neuroprotection: Design, synthesis, molecular modelling studies and biological activity. Antioxidants 15. https://doi.org/10.3390/antiox15030346.

Bonacorsi, S., Angeloni, L., Moliterno, M., Saito, G., Oddone, I., Secci, D., Raimondi, S., 2025. Channel-size enlarging strategy for liposome production scale-up: a simplified approach. Int. J. Pharm. 684. https://doi.org/10.1016/j.ijpharm.2025.126181.

Burkard, W.P., Bonetti, E.P., Da Prada, M., Martin, J.R., Polc, P., Schaffner, R., Scherschlicht, R., Hefti, F., Müller, R.K., Wyss, P.C., 1989. Pharmacological profile of moclobemide, a short-acting and reversible inhibitor of monoamine oxidase type a. J. Pharmacol. Exp. Ther. 248, 391–399. https://doi.org/10.1016/S0022-3565(25)23664-3.

Buttitta, G., Bonacorsi, S., Barbarito, C., Moliterno, M., Pompei, S., Saito, G., Oddone, I., Verdone, G., Secci, D., Raimondi, S., 2024. Scalable microfluidic method for tunable liposomal production by a design of experiment approach. Int. J. Pharm. 662. https://doi.org/10.1016/j.ijpharm.2024.124460.

Buttitta, G., Lavagna, L., Bonacorsi, S., Barbarito, C., Moliterno, M., Saito, G., Oddone, I., Verdone, G., Raimondi, S., Panella, M., 2025. Machine learning-guided microfluidic optimization of clinically inspired liposomes for nanomedicine applications. Int. J. Pharm. 686. https://doi.org/10.1016/j.ijpharm.2025.126362.

De Colli, M., Zara, S., Di Giacomo, V., Patruno, A., Marconi, G.D., Gallorini, M., Zizzari, V.L., Tetè, G., Cataldi, A., 2015. Nitric oxide-mediated cytotoxic effect induced by zoledronic acid treatment on human gingival fibroblasts. Clin. Oral Invest. 19, 1269–1277. https://doi.org/10.1007/s00784-014-1344-9.

A. Dean D. Voss D. Draguljić Design and Analysis of Experiments. Springer Texts in Statistics 2017 Springer International Publishing Cham 10.1007/978-3-319-52250-0.

Eugster, R., Ganguin, A.A., Seidi, A., Aleandri, S., Luciani, P., 2024a. 3D printing injectable microbeads using a composite liposomal ink for local treatment of peritoneal diseases. Drug Deliv. Transl. Res. 14, 1567–1581. https://doi.org/10.1007/s13346-023-01472-y.

Eugster, R., Orsi, M., Buttitta, G., Serafini, N., Tiboni, M., Casettari, L., Reymond, J.L., Aleandri, S., Luciani, P., 2024b. Leveraging machine learning to streamline the development of liposomal drug delivery systems. J. Control. Release 376, 1025–1038. https://doi.org/10.1016/j.jconrel.2024.10.065.

Eugster, R., Santschi, M., Buttitta, G., Olcay, B., Reymond, J.L., Aleandri, S., Luciani, P., 2025. 3D-printed cannabidiol stent for local treatment of urinary tract infections. Int. J. Pharm. 680. https://doi.org/10.1016/j.ijpharm.2025.125761.

Giakoumatos, E.C., Gascoigne, L., Gumí-Audenis, B., García, Á.G., Tuinier, R., Voets, I.K., 2022. Impact of poly(ethylene glycol) functionalized lipids on ordering and fluidity of colloid supported lipid bilayers. Soft Matter 18, 7569–7578. https://doi.org/10.1039/d2sm00806h.

Grassucci, R.A., Taylor, D.J., Frank, J., 2007. Preparation of macromolecular complexes for cryo-electron microscopy. Nat. Protoc. 2, 3239–3246. https://doi.org/10.1038/nprot.2007.452.

Guglielmi, P., Coluccia, M., Marconi, G.D., Ortuso, F., Procopio, F., Carradori, S., Pizzicannella, J., Arrighi, F., Troiani, A., Salvitti, C., Borges, F., Chavarria, D., Chimenti, P., Secci, D., Diomede, F., 2025. Design, synthesis, and biological activity of 2-aroylbenzofuran-3-ols and 2-aroylbenzofuran derivatives: a new route towards hMAO-B inhibition. Eur. J. Med. Chem. 297. https://doi.org/10.1016/j.ejmech.2025.117983.

Guglielmi, P., Secci, D., Petzer, A., Bagetta, D., Chimenti, P., Rotondi, G., Ferrante, C., Recinella, L., Leone, S., Alcaro, S., Zengin, G., Petzer, J.P., Ortuso, F., Carradori, S., 2019. Benzo[b]thiophen-3-ol derivatives as effective inhibitors of human monoamine oxidase: Design, synthesis, and biological activity. J. Enzyme Inhib. Med. Chem. 34, 1511–1525. https://doi.org/10.1080/14756366.2019.1653864.

He, C., Hu, Y., Yin, L., Tang, C., Yin, C., 2010. Effects of particle size and surface charge on cellular uptake and biodistribution of polymeric nanoparticles. Biomaterials 31, 3657–3666. https://doi.org/10.1016/j.biomaterials.2010.01.065.

Herdiana, Y., 2025. Bridging the gap: the role of advanced formulation strategies in the clinical translation of nanoparticle-based drug delivery systems. Int. J. Nanomed. https://doi.org/10.2147/IJN.S554821.

Hu, Y., Gaillard, P.J., de Lange, E.C.M., Hammarlund-Udenaes, M., 2019. Targeted brain delivery of methotrexate by glutathione PEGylated liposomes: how can the formulation make a difference? Eur. J. Pharm. Biopharm. 139, 197–204. https://doi.org/10.1016/j.ejpb.2019.04.004.

Iacovino, L.G., Magnani, F., Binda, C., 2018. The structure of monoamine oxidases: past, present, and future. J. Neural Transm. https://doi.org/10.1007/s00702-018-1915-z.

Junkes, L., Quagliato, L.A., Appolinario, J.C., Shader, R.I., Nardi, A.E., 2025. MAO inhibitors for treatment-resistant depression: Bringing an updated perspective on pioneering drugs. Pharmacol. Res. https://doi.org/10.1016/j.phrs.2025.107876.

Kim, T.T., Xu, C., Amsterdam, J.D., 2025. Comparison of effectiveness and side effects of selegiline transdermal system versus oral monoamine oxidase inhibitors and tricyclic antidepressants for treatment-resistant depression. J. Affect. Disord. 376, 47–51. https://doi.org/10.1016/j.jad.2025.02.003.

Kuntsche, J., Horst, J.C., Bunjes, H., 2011. Cryogenic transmission electron microscopy (cryo-TEM) for studying the morphology of colloidal drug delivery systems. Int. J. Pharm. https://doi.org/10.1016/j.ijpharm.2011.02.001.

Lee, C.Y., Tsai, T., Peng, P.C., Chen, C.T., 2022. Fabrication of doxorubicin-loaded lipid-based nanocarriers by microfluidic rapid mixing. Biomedicines 10. https://doi.org/10.3390/biomedicines10061259.

Lindsay, S., Tumolva, O., Khamiakova, T., Coppenolle, H., Kovarik, M., Shah, S., Holm, R., Perrie, Y., 2024. Can we simplify liposome manufacturing using a complex DoE approach? Pharmaceutics 16. https://doi.org/10.3390/pharmaceutics16091159.

Ling, D., Li, N., Pan, X., Gao, W., Li, H., Tian, Q., Li, J., Cheng, Q., Tang, L., Zhang, J., Gao, P., Ying, B., Wang, C., 2026. A new type of lipid nanoparticles with sphingomyelin-induced active lipid raft structures for improved mRNA cellular uptake. J. Control. Release 391. https://doi.org/10.1016/j.jconrel.2026.114640.

Lou, G., Anderluzzi, G., Woods, S., Roberts, C.W., Perrie, Y., 2019. A novel microfluidic-based approach to formulate size-tuneable large unilamellar cationic liposomes: Formulation, cellular uptake and biodistribution investigations. Eur. J. Pharm. Biopharm. 143, 51–60. https://doi.org/10.1016/j.ejpb.2019.08.013.

Marconi, G.D., Carradori, S., Ricci, A., Guglielmi, P., Cataldi, A., Zara, S., 2019. Kinesin Eg5 targeting inhibitors as a new strategy for gastric adenocarcinoma treatment. Molecules 24. https://doi.org/10.3390/molecules24213948.

Marconi, G.D., Della Rocca, Y., Fonticoli, L., Melfi, F., Rajan, T.S., Carradori, S., Pizzicannella, J., Trubiani, O., Diomede, F., 2022. C-Myc expression in oral squamous cell carcinoma: Molecular mechanisms in cell survival and cancer progression. Pharmaceuticals 15. https://doi.org/10.3390/ph15070890.

Monopoli, M.P., Åberg, C., Salvati, A., Dawson, K.A., 2012. Biomolecular coronas provide the biological identity of nanosized materials. Nat. Nanotechnol. 7, 779–786. https://doi.org/10.1038/nnano.2012.207.

Naoi, M., Maruyama, W., Shamoto-Nagai, M., 2022. Neuroprotective function of rasagiline and selegiline, inhibitors of type B monoamine oxidase, and role of monoamine oxidases in synucleinopathies. Int. J. Mol. Sci. https://doi.org/10.3390/ijms231911059.

Nele, V., Liguoro, D., Campani, V., Angelillo, A., Frigerio, R., Ortolano, A., Mancini, R., Fattore, L., De Rosa, G., Ciliberto, G., 2024. Self-assembling nanoparticles for miRNA

delivery towards precision medicine against melanoma. J. Drug Deliv. Sci. Technol. 101. https://doi.org/10.1016/j.jddst.2024.106169.
Niemelä, P., Hyvönen, M.T., Vattulainen, I., 2004. Structure and dynamics of sphingomyelin bilayer: Insight gained through systematic comparison to phosphatidylcholine. Biophys. J . 87, 2976–2989. https://doi.org/10.1529/biophysj.104.048702.
Nsairat, H., Khater, D., Sayed, U., Odeh, F., Al Bawab, A., Alshaer, W., 2022. Liposomes: Structure, composition, types, and clinical applications. Heliyon. https://doi.org/10.1016/j.heliyon.2022.e09394.
Pamunuwa, G., Karunaratne, V., Karunaratne, D.N., 2016. Effect of lipid composition on in vitro release and skin deposition of curcumin encapsulated liposomes. J. Nanomater. 2016. https://doi.org/10.1155/2016/4535790.
Rahman, M.S., Uddin, M.S., Rahman, M.A., Samsuzzaman, M., Behl, T., Hafeez, A., Perveen, A., Barreto, G.E., Ashraf, G.M., 2021. Exploring the role of monoamine oxidase activity in aging and Alzheimer's disease. Curr. Pharm. Des. 27, 4017–4029. https://doi.org/10.2174/1381612827666210612051713.
Rahnfeld, L., Luciani, P., 2020. Injectable lipid-based depot formulations: where do we stand? Pharmaceutics. https://doi.org/10.3390/pharmaceutics12060567.
Ramstedt, B., Slotte, J.P., 1999. Interaction of cholesterol with sphingomyelins and acyl-chain-matched phosphatidylcholines: a comparative study of the effect of the chain length. Biophys. J . 76, 908–915. https://doi.org/10.1016/S0006-3495(99)77254-1.
Rebollo, R., Oyoun, F., Corvis, Y., El-Hammadi, M.M., Saubamea, B., Andrieux, K., Mignet, N., Alhareth, K., 2022. Microfluidic manufacturing of liposomes: Development and optimization by design of experiment and machine learning. ACS Appl. Mater. Interfaces 14, 39736–39745. https://doi.org/10.1021/acsami.2c06627.
Roberts, S.A., Lee, C., Singh, S., Agrawal, N., 2022. Versatile encapsulation and synthesis of potent liposomes by thermal equilibration. Membranes 12. https://doi.org/10.3390/membranes12030319.
Roces, C.B., Port, E.C., Daskalakis, N.N., Watts, J.A., Aylott, J.W., Halbert, G.W., Perrie, Y., 2020. Rapid scale-up and production of active-loaded PEGylated liposomes. Int. J. Pharm. 586. https://doi.org/10.1016/j.ijpharm.2020.119566.
Roveri, M., Pfohl, A., Jaaks, P., Alijaj, N., Leroux, J.C., Luciani, P., Bernasconi, M., 2017. Prolonged circulation and increased tumor accumulation of liposomal vincristine in a mouse model of rhabdomyosarcoma. Nanomedicine 12, 1135–1151. https://doi.org/10.2217/nnm-2017-0430.
Santin, Y., Resta, J., Parini, A., Mialet-Perez, J., 2021. Monoamine oxidases in age-associated diseases: New perspectives for old enzymes. Ageing Res. Rev. https://doi.org/10.1016/j.arr.2021.101256.
Sedighi, M., Sieber, S., Rahimi, F., Shahbazi, M.A., Rezayan, A.H., Huwyler, J., Witzigmann, D., 2019. Rapid optimization of liposome characteristics using a combined microfluidics and design-of-experiment approach. Drug Deliv. Transl. Res. 9, 404–413. https://doi.org/10.1007/s13346-018-0587-4.
Shaldam, M.A., Carradori, S., Balaha, M., Guglielmi, P., Diomede, F., D'Agostino, I., Tawfik, H.O., 2026. Patents involving monoamine oxidase (MAO): a comprehensive update (2022–2025) on its inhibitors and applications. Expert Opin. Ther. Pat. https://doi.org/10.1080/13543776.2026.2633345.
Silverman, J.A., Deitcher, S.R., 2013. Marqibo® (vincristine sulfate liposome injection) improves the pharmacokinetics and pharmacodynamics of vincristine. Cancer Chemother. Pharmacol. https://doi.org/10.1007/s00280-012-2042-4.
Suk, J.S., Xu, Q., Kim, N., Hanes, J., Ensign, L.M., 2016. PEGylation as a strategy for improving nanoparticle-based drug and gene delivery. Adv. Drug Deliv. Rev. https://doi.org/10.1016/j.addr.2015.09.012.
Thevenot, J., Troutier, A.L., David, L., Delair, T., Ladavière, C., 2007. Steric stabilization of lipid/polymer particle assemblies by poly(ethylene glycol)-lipids. Biomacromolecules 8, 3651–3660. https://doi.org/10.1021/bm700753q.
Tipton, K.F., 2018. 90 years of monoamine oxidase: some progress and some confusion. J. Neural Transm. https://doi.org/10.1007/s00702-018-1881-5.
Wibroe, P.P., Ahmadvand, D., Oghabian, M.A., Yaghmur, A., Moghimi, S.M., 2016. An integrated assessment of morphology, size, and complement activation of the PEGylated liposomal doxorubicin products Doxil®, Caelyx®, DOXOrubicin, and SinaDoxosome. J. Control. Release 221, 1–8. https://doi.org/10.1016/j.jconrel.2015.11.021.